RESEARCH ARTICLE

WILEY

Assessment of groundwater recharge processes through karst vadose zone by cave percolation monitoring

Amaël Poulain[1] [iD] | Arnaud Watlet[2,3] [iD] | Olivier Kaufmann[2] | Michel Van Camp[3] [iD] | Hervé Jourde[4] | Naomi Mazzilli[5] [iD] | Gaëtan Rochez[1] | Romain Deleu[1] | Yves Quinif[2] | Vincent Hallet[1]

[1] University of Namur—Rue de Bruxelles, n°61, Namur B-5000, Belgium

[2] University of Mons—Rue de Houdain, n°9, Mons B-7000, Belgium

[3] Royal Observatory of Belgium—Avenue Circulaire, n°3, Uccle B-1180, Belgium

[4] Hydrosciences Montpellier—Avenue Professeur Emile Jeanbreau, n°300, Montpellier F-34090, France

[5] Université d'Avignon et des Pays de Vaucluse, UMR 1114 EMMAH—Rue Baruch de Spinoza, n°301, Avignon F-84000, France

Correspondence
Amaël Poulain, University of Namur, Rue de Bruxelles, n°61, Namur B-5000, Belgium.
Email: amael.poulain@unamur.be

Funding information
Fund for Scientific Research of Belgium, Grant/Award Number: T.0062.13

Abstract

Recharge processes of karst aquifers are difficult to assess given their strong heterogeneity and the poorly known effect of vadose zone on infiltration. However, recharge assessment is crucial for the evaluation of groundwater resources. Moreover, the vulnerability of karst aquifers depends on vadose zone behaviour because it is the place where most contamination takes place. In this work, an in situ experimental approach was performed to identify and quantify flow and storage processes occurring in karst vadose zone. Cave percolation monitoring and dye tracing were used to investigate unsaturated zone hydrological processes. Two flow components (diffuse and quick) were identified and, respectively, account for 66% and 34% of the recharge. Quickflow was found to be the result of bypass phenomenon in vadose zone related to water saturation. We identify the role of epikarst as a shunting area, most of the storage in the vadose zone occurring via the diffuse flow component in low permeability zones. Relationship between rainfall intensity and transit velocity was demonstrated, with 5 times higher velocities for the quick recharge mode than the diffuse mode. Modelling approach with KarstMod software allowed to simulate the hybrid recharge through vadose zone and shows promising chances to properly assess the recharge processes in karst aquifer based on simple physical models.

KEYWORDS

cave monitoring, dye tracing, epikarst, groundwater recharge, karst aquifer, stalactite drip, vadose zone

1 | INTRODUCTION

The role of the vadose zone regarding groundwater recharge is a key element when considering karst aquifers. The question of recharge and transfer through the vadose zone must be addressed when dealing with karst modelling for sustainable groundwater management (Hartmann, Goldscheider, Wagener, Lange, & Weiler, 2014; Hartmann, Lange, Weiler, Arbel, & Greenbaum, 2012; Tritz, Guinot, & Jourde, 2011). In particular, the fate of autogenic diffuse recharge and contamination regarding heterogeneous karst features needs to be

quantified considering the variability of flow conditions in karst (Bakalowicz, 1995). More generally, the vadose zone is important given its location at the transition between the surface and the water table, and because it represents an important support for vegetation and fauna development (Figure 1).

Many field studies allowed to describe the functions of karst vadose zone and in particular its importance with respect to aquifer recharge. Biological, hydrogeological, and geomorphological aspects and functions of vadose zones were identified (Bakalowicz, 2013; Bakalowicz, Blavoux, & Mangin, 1974; Klimchouk, 2004; Mangin,
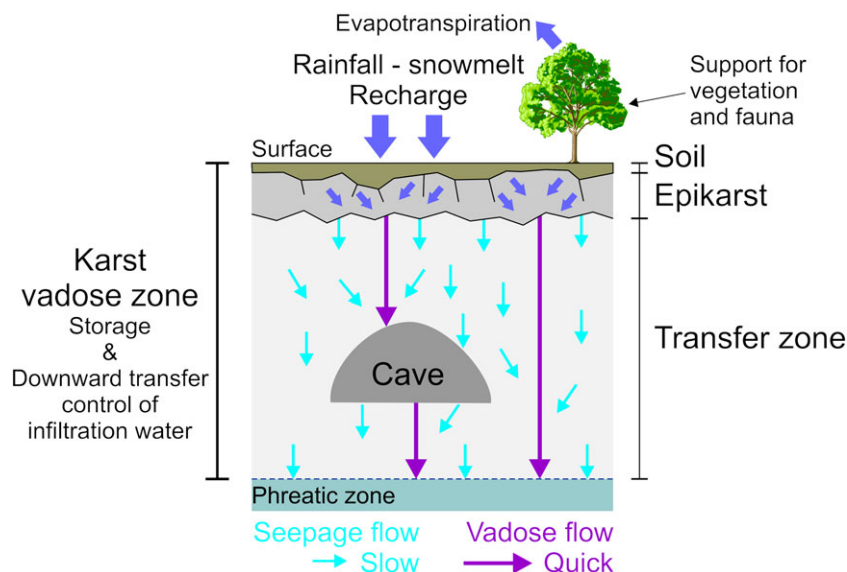
FIGURE 1 Overview of the vadose zone main components (soil, epikarst, and transfer zone) and roles in the superficial part of karst aquifer

1975; Rouch, 1964, 1968; Smart & Friederich, 1987; Williams, 1983, 2008) and highlighted its crucial role in the karst system. Since then, several experimental approaches focused on the importance of vadose zone regarding karst groundwater dynamic (Aquilina, Ladouche, & Doerfliger, 2005; Arbel, Greenbaum, Lange, & Inbar, 2010; Bakalowicz, 1979; Deville, 2013; Jacob et al., 2008; Kogovsek, 2010; Perrin, 2003; Pronk, Goldscheider, Zopfi, & Zwahlen, 2009; Trcek, 2005). Karst researchers agree that the vadose zone plays a major role to regulate the aquifer recharge. This recharge regulation function can be divided into storage and downward transfer control of water.

The storage role of vadose zone is its most important feature and is related to the concept of epikarst. The epikarst (Bakalowicz, 2013; Mangin, 1975; Williams, 1983, 2008) refers to a superficial layer of enhanced permeability and porosity in the vadose zone. Due to its characteristics, a nonpermanent, discontinuous, and perched storage of water may occur in the epikarst (Ford & Williams, 2007; Jones, Culver, & Herman, 2004). This storage function is responsible for the delay, mixing, and dilution of recharge as well as the sustained alimentation of vadose percolation during droughts (Baker & Brunsdon, 2003; Genty & Deflandre, 1998; Pipan & Culver, 2007; Poulain, Rochez, Bonniver, & Hallet, 2015; Smart & Friederich, 1987). In certain cases, vadose storage is assumed to be the main component of karst spring discharge (Aquilina, Ladouche, & Doerfliger, 2006; Mudarra & Andreo, 2011; Trcek, 2007).

Spatial heterogeneities associated to epikarst control and divide water infiltration towards the phreatic zone. This function has been evidenced by variable vadose flow regimes in reaction to precipitation (Mangin, 1975; Smart & Friederich, 1987). Flow regimes into caves can be separated into two extreme types: seepage and vadose flow. These extremes illustrate two modes of infiltration transfer through vadose zone and have been reported in several field studies (Markowska et al., 2015; Perrin, 2003; Perrin & Kopp, 2005; Pronk et al., 2009; Sauter, 1992; Trcek, 2005). The seepage mode, often described as diffuse flow, represents the transfer through low permeability parts of the vadose zone and can be related to the drainage of the epikarstic storage. This transfer mode is generally identified as the slow subsystem of recharge (Sauter, 1992). The second mode is the

vadose flow, also described as shaft flow. It represents the quick component of recharge through fractures and shafts. These sites of concentrated flow are the fastest routes for the transmission of autogenic recharge (Gunn, 1983; Williams, 2008). However, a saturation threshold is generally necessary to allow vadose connectivity. This saturation activates shafts and open fractures and allows fast transfer of infiltration. This was observed in many study cases and described as a bypass flow (Arbel et al., 2010; Perrin, 2003; Sheffer et al., 2011; Tritz et al., 2011). Quickflow is ephemeral because the high permeability routes allow fast drainage of the recharge and will quickly dry up. Given the strong heterogeneity of karst features inherited from lithology, fractures, and karstogenesis, recharge processes in a given place will comprise a continuum between seepage recharge through low permeability zones and quickflow through fractures and open shafts. Diversity in percolation regimes reflects this continuum, and most of the vadose percolations exhibit a mixed behaviour (Jeannin, Groves, & Häuselaman, 2007).

The variability of recharge mode through karst vadose zone was further described using the response of natural and artificial tracers at depth. Smart and Friederich (1987) show importance of lateral movements and the influence of saturation state on infiltration processes. Bottrell and Atkinson (1992), Kogovsek (1997, 2010), and Kogovsek and Petric (2014) identified recharge flow components and their residence time in the vadose zone. Pronk et al. (2009) used artificial tracers and particles to detail the recharge process and role of epikarst regarding contamination attenuation. Perrin (2003) identified the importance of dynamic storage in the epikarst and its role in the regulation of recharge between slow and fast flows. Trcek (2005) pointed out the duality of recharge and the residence time of vadose flow components.

To synthetize the role of vadose zone, the epikarst concentrates quickflow towards the most permeable part of the vadose zone, whereas a slow recharge component is stored in less permeable parts (Klimchouk, Sauro, & Lazzarotto, 1996). In addition, vadose zone transfers the recharge from the surface to the phreatic zone in two ways: quickflow through fractures or open shafts and slow seepage through matrix (Trcek, 2005). The relative importance of vadose storage and modes of transfers depends upon the intensity of recharge

and the saturation state of the system for a given geological context and system geometry (Jocson, Jenson, & Contractor, 2002).

This model for karst vadose zone prevails in the karst community. Nevertheless, as the hydrological functions of vadose zone are identified, one question remains. It concerns the quantification of their impact on the recharge effectiveness and the vulnerability of karst groundwater. How do these relative modes of recharge and storage influence groundwater in quantitative and qualitative ways?

This study considers vadose zone as a whole, including soil, epikarst, and transfer zone (Figure 1). Here, we will focus on functions (transfer and storage) and quantification of these functions. In this paper, experimental methodologies were applied to the vadose zone of the Rochefort Cave in Belgium. Based on percolation discharge, physico-chemical analysis and dye tracing, the variable recharge components of the percolation, were identified. This enabled the quantification of recharge modes in the infiltration dynamic. We also characterize the recharge modes, and this helps to understand how they contribute in the aquifer recharge and influence aquifer vulnerability.

2 | STUDY AREA

The Rochefort Cave is located in southern Belgium and is part of the Wamme–Lomme karst system (Figure 2a; Poulain et al., 2017). This active karst is developed in Givetian limestones of the Variscan fold-and-thrust belt. Givetian rocks in this part of Belgium are mainly composed of biostromal limestones (Bultynck & Dejonghe, 2001; Willems, Ek, & Marion, 2011). Those folded and fractured Devonian limestones host the main karst features of the country.

The local geology consists in an overturned series of limestone beds, with 40–50° south dipping strata striking N70°E. This Givetian series is 450 m thick with alternating massive limestones and smaller clayey beds. The average bed thickness is 0.3 to 1 m. The Rochefort Cave is the main cave of the area with 6.6 km of galleries (Figure 2b).

The studied percolation is located in the Val d'Enfer, the main chamber of the Rochefort Cave (Figure 2b,c). This chamber is 60 m long, 45 m wide, and 15 m high. The limestone layer between the surface and cave roof is between 20 and 30 m thick. The rocks sequence visible in the chamber is mainly composed by thick (>1 m) beds of massive limestone. Two sequences of finely bedded (10–20-cm beds) limestones can be found (Figure 2c). Those limestones are highly fractured compared to the adjacent massive limestone and show lower $CaCO_3$ contents (50–80% $CaCO_3$ with an average content of 70%, value is >80% for massive limestone). They appear more weathered and porous than the massive limestone. The description of the lithology sequence is presented in Figure S1.

Percolation in the chamber roof is visible in several open shafts in the massive limestone. However, the majority of the percolation is observed in the clayey limestones sequences. Moreover, percolation in those sequences is perennial, whereas percolation in open shafts of the massive limestone is mainly active after rainfall events. For this study, a percolation coming from a fracture in the clayed limestone sequence was chosen because of its sustained discharge through the year. It was expected that fractures and weathering in clayed limestones influence the percolation behaviour. The monitoring focuses on a single percolation point to get a punctual quantitative information (discharge and quantitative dye tracing) rather than integrated measurement (drip collection).

The surface topography over the cave is mainly flat and covered by deciduous trees (hornbeams, limes, oaks, and hazels), roads, and a few buildings. The soil layer is thin (10–40 cm) and has a high limestone gravel load (50% to 80%). Picture of the cave environment is available in Figure S2.

South Belgium has a temperate climate with fresh and wet summer followed by mild and rainy winters. The average annual precipitation is 824 mm, and average temperature is 10.9 °C (Royal Meteorological Institute data 2008–2014). For 2016, rainfall was evenly distributed along the year (minimum of 0, maximum of 49 mm/day) with an average of 2.2 mm/day. Evapotranspiration
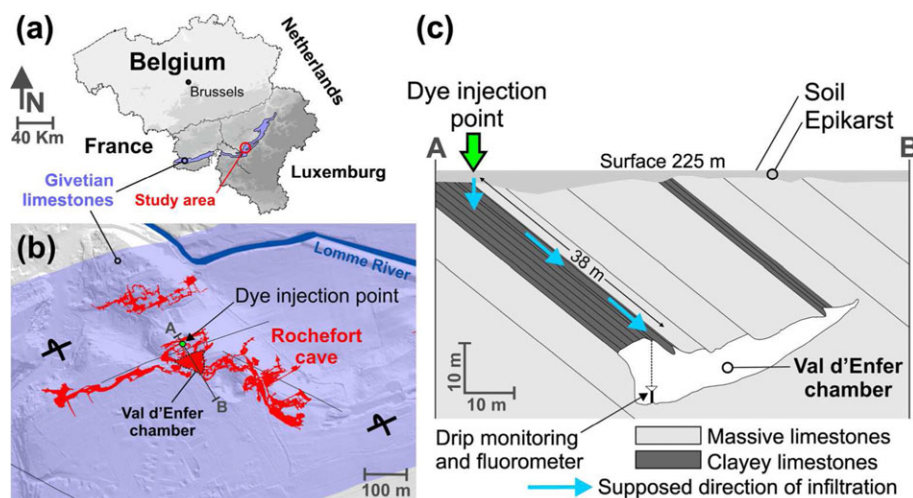
FIGURE 2 (a) Location map of the study area in Givetian limestones of South Belgium, (b) map of the Rochefort Cave in Givetian limestones (Barchy, Dejonghe, & Marion, 2014) with location of the Val d'Enfer chamber, dye tracing injection point and cross-section A–B, and (c) cross-section A–B through the Givetian limestone vadose zone with the Val d'Enfer chamber, location of dye injection, and percolation monitoring (cave topographies by Triantafyllou, Watlet, Kaufmann, & Le Mouélic, 2016; Birkhoff et al., 2013; Legros, 2000; Quinif & Vandycke, 2001; Dehove, Nandance, & Renier, 1978; De Block, 1972)

calculated with the Penman–Monteith methodology fluctuates from zero during winter to 5.4 mm/day in July (Allen, Pereira, Raes, & Smith, 1998). Given the specific condition of infiltration in karst, effective rainfall (P-ETP) was considered as the input signal for infiltration in the system (Figure 3). One snowfall event was recorded during this study, in March 2016.

3 | METHODOLOGY

3.1 | Meteorological data

Rainfall and air temperature were sampled every minute above the cave. The temperature was measured with a Campbell T10 probe with a 0.03 °C resolution and 0.03 °C precision. Rainfall and snow were gauged in a Lufft tipping bucket-type heated rain gauge with a 0.1-mm resolution. A second set of rainfall data recorded in a nearby station with a nonheated rain gauge was used to estimate the snow-melt (Pameseb asbl–Jemelle station, 1 km far from the cave). This other station also gives evapotranspiration data based on the Penman–Monteith method (Allen et al., 1998).

3.2 | Percolation water monitoring

The drip discharge monitoring is made of an auto-siphoning gauge with capacitive sensors and was designed by University of Mons based on an original prototype from the Royal Observatory of Belgium (Kaufmann, Bastin, Barcella, Watlet, & Van Ruymbeke, 2016; Figure S3). An electrical conductivity (EC) measurement is made with a Campbell CS547A probe (accuracy of ±5%). In addition, the drip-water temperature was measured with a Fluo-Green fluorometer (Poulain et al., 2017) during the dye tracing experiment to allow comparisons with surface temperature.

3.3 | Hydrograph separation using the master recession curve

The subregimes of flow measured in the percolation were separated using the methodology described by Malik (2015) based on the master recession curve (MRC). The method comes from the analytical solution describing aquifer recession segments developed based on the Maillet (1905) equation.

$$Q_t = Q_0 e^{-\alpha t}, \tag{1}$$

where Q_0 is the initial discharge, Q_t is the discharge at time t, and α is the recession coefficient in (day^{-1}). The model of Kullman (1990) can be alternatively used to describe the linear recession observed for the quickflow component. Factor β is the recession coefficient for quickflow.

$$Q_t = \left(\frac{1}{2} + \frac{|1-\beta t|}{2(1-\beta t)}\right)Q_0(1-\beta t). \tag{2}$$

Each recession limb is approximated by a function that is the sum of several exponential or linear segments of the total recession, also described as the MRC (Malik, 2015).

$$Q_t = \sum_{i=1}^{n} Q_{0i} e^{-\alpha_i t} + \sum_{j=1}^{m} \left(\frac{1}{2} + \frac{|1-\beta_j t|}{2(1-\beta_j t)}\right)Q_{0j}(1-\beta_j t). \tag{3}$$

The MRC is calculated for every recession measured in the percolation discharge. It allows identifying and quantifying the different flow components of the percolation based on their recession properties.

3.4 | Surface to cave dye tracing

The injection location was chosen following the limestone dipping (40° to the south) as the infiltration is likely to follow the bedding planes (Figure 2). This dipping effect on vadose infiltration was previously shown in the same geological context (Poulain et al., 2015). Five
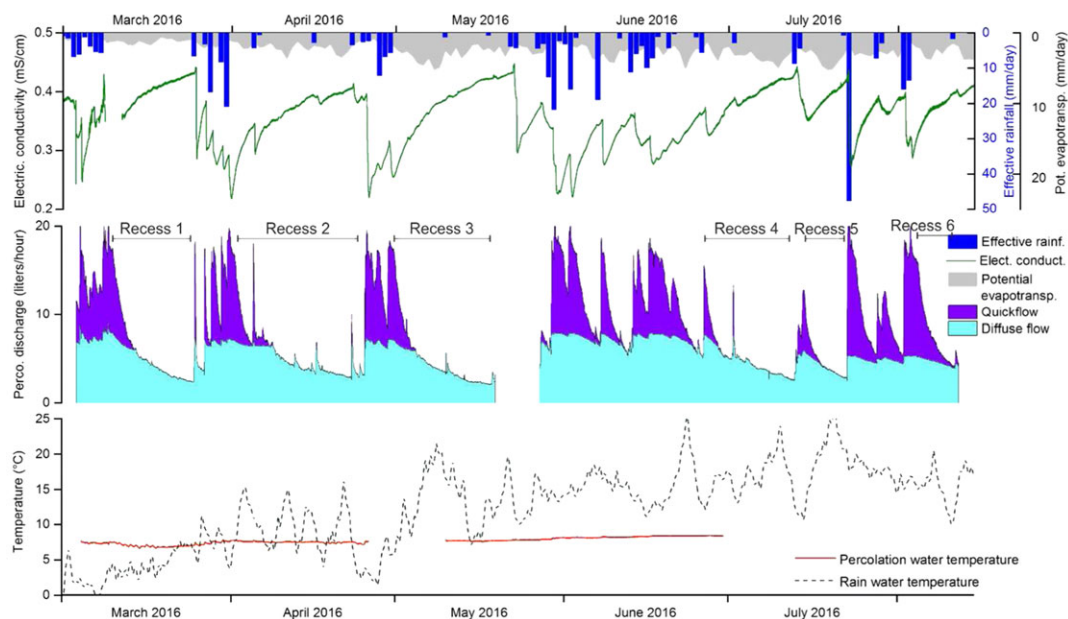
FIGURE 3 Field results of the Rochefort Cave percolation monitoring in 2016 with daily effective rainfall and potential evapotranspiration, percolation water electrical conductivity, percolation and rain water temperature, and percolation discharge. The discharge is separated in two flow types (quickflow and diffuse flow) according to the recession analysis based on the six main recession events of 2016 (Recess. 1–6)

hundred grams of uranine were injected on the ground above the cave on the March 4, 2016 at 4:15 p.m. The minimum distance between the injection point and the percolation is 38 m (Figure 2c). Kogovsek and Petric (2014) evidenced the influence of injection mode on the results of vadose dye tracing. To avoid misinterpretation, the injection has to be performed without any soil removing and using the minimum volume of water for dye dilution (40 L). A 20-cm diameter polyvinyl chloride pipe was used to guarantee the minimal injection area (Figure S3).

Drip-water temperature and tracer concentration were measured using a Fluo-Green field fluorometer. The compact device was placed above the discharge measurement in a small pool (5 L) collecting the drip water. Considering the size of the pool and the average percolation discharge (7 L/hr), this method has a negligible buffering effect on the measurements. The fluorimeter was calibrated at the University of Namur using blank sample and uranine. Resolution is 0.09 ppb for uranine and 0.06 °C for temperature (Poulain et al., 2017).

4 | FIELD RESULTS

### 4.1 | Infiltration dynamic through karst vadose zone

4.1.1 | Percolation discharge signal

The percolation in the Rochefort Cave shows an important variability at short time scale, but no superimposed long-term pattern was noticeable between March and August 2016. Discharge behaviour is similar at the end of winter and during summer (Figure 3). We note that the precipitations in June and July were unusually high in 2016 (226 vs. 123 mm in 2015), inducing a high amount of effective rainfall. According to the classification of Smart and Friederich (1987), the percolation is described as a vadose flow, between sustained seepage flow and ephemeral subcutaneous flow. The discharge shows both sharp reactions to effective rainfall events and sustained percolation during dry periods, arguing for highly conductive paths in relationship with storage.

As the relationship with effective rainfall is evident, it is not possible to identify the long-term variation of a storage that could be influenced by evapotranspiration. However, several drip monitoring studies evidenced the strong seasonal effect of evapotranspiration on vadose percolation (Smart & Friederich, 1987; Genty & Deflandre, 1998; Jocson et al., 2002; Sheffer et al., 2011; Kogovsek, 2010; Arbel et al., 2010; Kogovsek & Petric, 2014; Poulain et al., 2015; Fu et al., 2016). In this case, the reaction of the percolation to effective rainfall is almost identical through the observation period, and recession patterns are also similar. This could be explained by the land cover of the cave, including roads, a parking lot, and buildings. An umbrella effect caused by those constructions could result in a lower evapotranspiration over this area. Consequently, the regularity of recharge at this percolation point during 5 months represents an opportunity to focus on flow and storage characteristics of the vadose zone.

The discharge signal shows a very quick (1 to 3 hr) reaction to rainfall leading to a regular maximum discharge around 18–20 L/hr. The discharge peaks are similar along the period indicating a limited capacity of the drainage routes. Once rainfall stops, the discharge drops quickly with a two-component recession curve. Analysis of the recession components shows that they have similar characteristics. Figure 4 and Table 1 present data from six recession events observed in 2016 with initial discharge (Q_0), recession constant ($T_{1/3}$, time to reach one third of the initial discharge), and recession coefficient (α or β, slope of the recession curve). The recession constants are similar between events. The first component is almost linear with a recession constant of 1–2 days, whereas the second is exponential with a recession constant longer than 10 days.

A diffuse flow and quickflow subregimes were separated using the methodology described by Malik (2015) based on the MRC and using representative time of measured discharges. This method was used on the recessions of the percolation discharge and is described in the Section 3. Based on the MRC expression for the six recession events, every discharge of the hydrograph can be described by a representative time (time elapsed from the maximum discharge value).
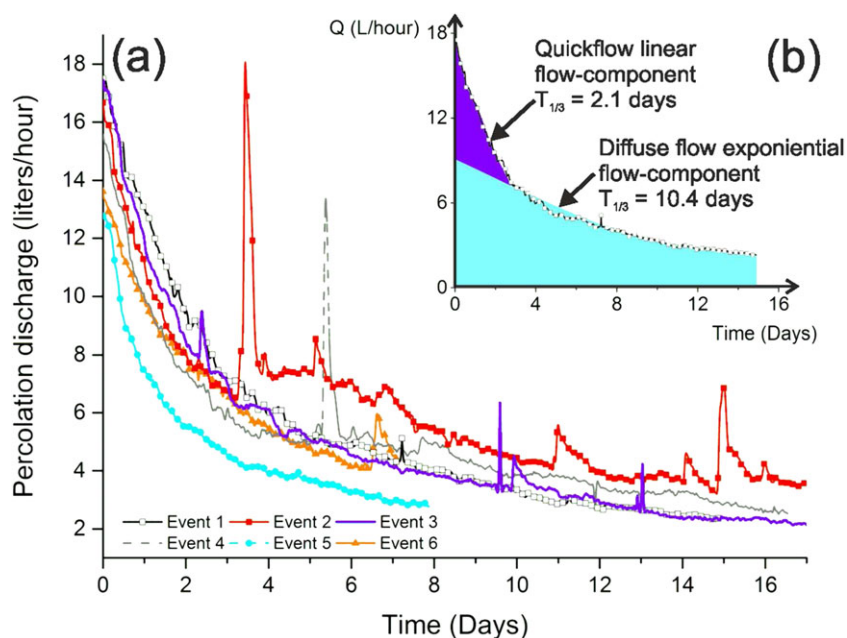
FIGURE 4 (a) The six recession events of the percolation discharge in 2016 and (b) delineation of differently shaped flow components of discharge on the recession of Event 1. Individual characteristics of each recession event are given in Table 1

TABLE 1 Characteristics of the six recession events of 2016 for the Val d'Enfer percolation

Recession event	Flow component	Initial discharge (L/hr)	Recession constant $T_{1/3}$ (days)	Recession coefficient α or β (days^{-1})
Event 1	Quickflow	8.72	2.1	2.80[a]
	Diffuse flow	7.88	10.4	0.085[b]
Event 2	Quickflow	8.67	1.5	3.99[a]
	Diffuse flow	6.98	18.3	0.041[b]
Event 3	Quickflow	9.68	1.7	3.82[a]
	Diffuse flow	7.03	15.4	0.071[b]
Event 4	Quickflow	9.56	1.1	0.95[b]
	Diffuse flow	7.82	16.7	0.056[b]
Event 5	Quickflow	7.21	0.9	1.18[b]
	Diffuse flow	5.88	11.7	0.097[b]
Event 6	Quickflow	8.21	2.2	0.49[b]
	Diffuse flow	5.13	32.1	0.034[b]

[a]β = linear recession.

[b]α = exponential recession.

Using this representative time in individual flow-components equations allows the quantification of these flow components. Figure 3 displays the flow components separation result for the entire hydrograph (quickflow and diffuse flow). This approach uses simplified assumptions of aquifer properties and the related hydrological processes. Nevertheless, it is generally used for karst springs because it allows a gross estimation of flow components (Malik, 2015). Here, the model was applied to vadose zone flow given the regularity of discharge reactions through the year reflecting vadose storage and transmission properties in a well-defined system. Differences between flow components are caused by the vadose zone processes and seem suited to quantify the recharge functions.

The diffuse—or slow—flow component shows a regular discharge (mean discharge of 5.31 L/hr with standard deviation [SD] of 1.66). The maximum calculated discharge is 8.9 L/hr, whereas minimum is around 2.0 L/hr after extended dry period. The total volume of this flow component over the studied period is 20,140 L, representing 66% of the total percolation discharge. This means that recharge through the vadose zone at this point is mainly driven by slow infiltration.

The quickflow component shows an irregular pattern with sharp increase of discharge (mean = 4.89 L/hr, SD = 2.79) but also quick recession. The flow stops a few days after the rainfall as highlighted by the low recession constant. The total volume is 10,035 L, representing 34% of the total percolation discharge.

4.1.2 | EC signal

EC monitoring of percolation water (Figure 3) shows a regular behaviour of hydrochemistry changes due to recharge. EC has a mean value of 360 μS/cm with maximum of 470 μS/cm and minimum of 220 μS/cm. Variations of EC in the percolation water mimic observations in karst springs (Hunkeler & Mudry, 2007). During periods without significant recharge, EC values tend to reach high values, here, ranging around 450 μS/cm. This high value represents the chemical signature of the vadose storage water that has the longer residence time in the system. When a recharge event occurs, a short piston effect is observed with a quick increase of the EC (+10 μS/cm). This highlights a limited transfer of the storage water in the vadose zone by a

pressure pulse. After this increase, EC drops quickly to low values between 220 and 300 μS/cm. This is caused by the arrival of freshly infiltrated water at the percolation. As soon as this input stops, the EC gradually increase in the absence of recharge event. These variations of EC are typical in karst and reflect a two-poles mixing behaviour between freshly infiltrated water and water that is stored in the vadose zone since previous events.

4.1.3 | Percolation water temperature signal

Percolation water temperature is highly buffered when arriving in the cave compared with surface temperature (Figure 3). A few hours transit in the vadose zone enables an advanced thermal equilibrium between water and cave. Moreover, because the measurement is made in a small pool (not on the drip itself), the amplitude of the temperature variations is damped. However, this does not affect the dynamic of the temperature, which can be interpreted.

Mean temperature of the percolation water is 7.7 °C with SD = 0.46 °C, whereas surface mean temperature is 10.7 °C with SD = 5.98 °C. Figure 5 shows temperature variability during 1 month
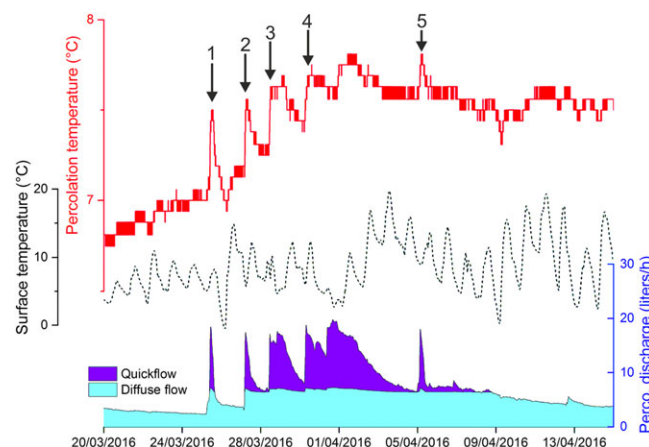
FIGURE 5 Details of the surface (black dashed line) and percolation water temperature (red line) in front of the percolation discharge and the two flow components. Note the different Y axis for the temperature plots. Black arrows represent the effect of quickflow transit on the percolation temperature

in 2016. Whereas the percolation water shows almost no seasonal variability on the Figure 3, daily cycles are observed at the sensor resolution (0.05 °C) on the Figure 5. Those cycles lag surface ones by 3 to 6 hr. During rainfall events, the percolation temperature changes synchronously with the discharge indicating a faster transit that is less damped by mixing or prolonged residence time (Figure 5).

## 4.2 | Dye tracing in the vadose zone

4.2.1 | General analysis

Figure 6 and Table 2 summarize the results of the vadose dye tracing. First detection of uranine occurred 3.75 hr after injection, giving a maximum velocity of 10.25 m/hr. This represents the minimal transit time in the vadose zone without rainfall or significant flush of the dye. As previously shown in similar context (Poulain et al., 2015), bedding planes are a preferential pathway for infiltration. The breakthrough curve (BTC) is quite complex with a multimodal behaviour and a total restitution time of more than 120 days.

The first hours of tracer breakthrough show a slow increase of concentration up to 40 ppb (Figure 6a). After 15 hr, a sharp break is observed in the BTC with a quick increase of the concentration up

to 225 ppb. This peak is associated with a rainfall event and an increase in the percolation discharge. Fifteen to twenty hours after the rainfall event, the concentration quickly decreases to around 60 ppb. Such rainfall-associated peaks are visible at least 16 times during the restitution period (Figure 6b). This forms a secondary restitution mode arguing for a multicomponent flow. As suggested by Sinreich and Flynn (2011) and Behrens et al. (1992), solute breakthrough can be split into partial BTCs representing separate flow paths. On the first hand, the slow first arrival and a retarded transit mode may be caused by the diffuse flow. On the other hand, quickflow could result in a fast but discontinuous mode of transit superimposed to the first one. The separation of the BTC into two recharge modes has been made by removing the low frequency trend (Figure 6c) that is measured at the beginning of the BTC (the slow increase during the first 15 hr) and that is visible between the secondary restitution peaks. By removing this background restitution, 16 secondary restitution peaks remained (Figure 6d). The two recharge modes may be described as follows:

- The first mode of transport results in a unimodal BTC with a maximum velocity around 10 m/hr. Peak arrival time indicates
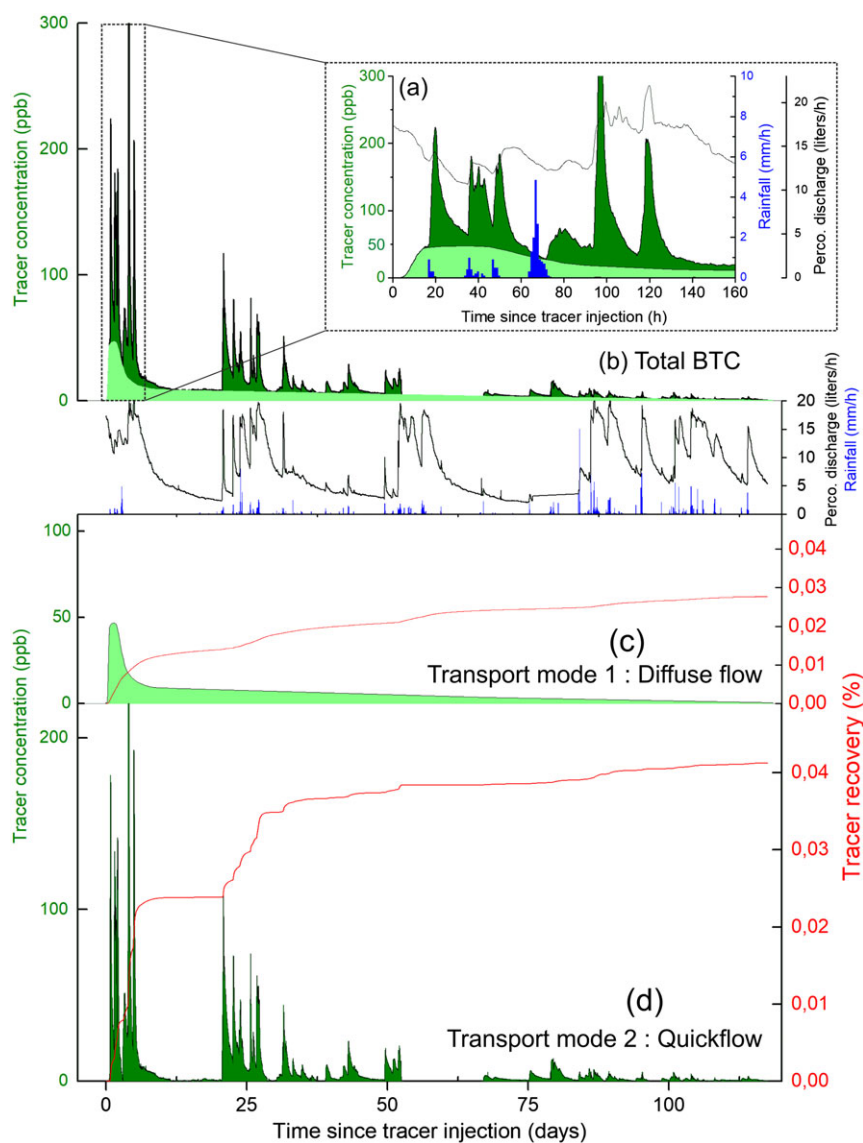
FIGURE 6 Breakthrough curve (BTC) of the vadose dye tracing above the Val d'Enfer chamber with (a) total BTC for the first 160 hr after tracer injection showing the first arrival and the rainfall events that caused secondary peaks of dye, (b) total BTC for the entire restitution period, the two transport modes are illustrated by two distinct colours, (c) partial BTC representing the first transport mode associated with diffuse flow recharge, and (d) partial BTC representing the second transport mode associated with quickflow recharge

TABLE 2 Main characteristics of the vadose dye tracing breakthrough curve (BTC) separated into two transport modes through the vadose zone (x̄ = mean value; RR = Recovery Rate)

	First arrival (hr)	Peak time (hr)	Max tracer concen. (ppb)	Max velocity (m/hr)	Peak velocity (m/hr)	Total restitution time (hr)	RR (%)
Transport mode 1: Diffuse flow	3.75	20–40	45–55	10	1–2	+2,500	0.028 (40% of recovered dye)
Transport mode 2: Quickflow	0.68–3.78 (x̄ = 1.48)	2.1–7.7 (x̄ = 4.2)	225–4 decrease over time	10–55 (x̄ = 25.7)	4.9–17.9 (x̄ = 9.0)	15–50	0.041 (60% of recovered dye)
Total BTC							0.069

dominant flow velocities in the range of 1–2 m/hr, at low concentration (peak of 45 to 55 ppb). The long tailing constitutes the baseline between secondary peaks and highlights significant retardation. This mode is related to the diffuse infiltration of water through the vadose zone;

- A second mode of transport is linked to surface rainfall events and quickflow that generate short pulses secondary BTCs. Those BTCs result from remobilization of dye trapped in the vadose zone by quickflow. This mode is faster when considering the time of rainfall and the time of the dye concentration anomaly at the percolation (maximum velocity between 10 and 55 m/hr). Dye is more concentrated (up to 250 ppb), and retardation is less effective, resulting in sharp BTC that are super imposed to the first transport mode.

The total recovery based on dye concentration and percolation discharge is 0.345 g. It means less than 0.07% of the injected mass. The recovery rates (RR) for diffuse flow and quickflow are 40% and 60% of the total recovered dye, respectively.

4.2.2 | Quickflow BTCs analysis

The 16 secondary BTCs precise the quickflow transit through the vadose zone. The peak concentration gradually decreases over time, indicating a defined amount of trapped dye which is gradually leached (Bottrell & Atkinson, 1992). Concentration does not depend of rainfall intensity or vadose zone conditions of saturation as observed by Kogovsek and Petric (2014). This indicates that the high permeability routes, once activated, drain a defined volume of the vadose zone. When maximum tracer concentrations are normalized on a 0 to 1 scale

(Figure 7a), individual BTCs exhibit similar characteristics in terms of first arrival, peak time, and total restitution time. Therefore, mean first arrival, mean peak time, and mean total restitution time allow to draw an average BTC showing the typical behaviour of the fast mode transport through the vadose zone (Figure 7b). Mean first arrival is 1.5 hr, giving a maximum velocity of 25.7 m/hr. Mean peak time of 4.2 hr indicates a dominant velocity of 9.0 m/hr. Transit of recharge with the quickflow mode is up to 5 times faster than the diffuse mode without rainfall effect.

Three secondary peaks, measured 80, 100, and 120 hr after the tracer injection (Figures 6a and 8), differ significantly from this analysis. Those peaks are due to the snowmelt of a 14-mm snowfall as recorded by the nonheated rain gauge. The melting of the snow during the two following days caused a higher tracer restitution with concentration up to 340 ppb (Figure 8). The third peak is more than likely also caused by snowmelt even if the nonheated rain gauge did not record the melting. This is probably due to local variability in the snow cover between the rain gauge and the ground. These data suggest that recharge caused by snowmelt has a different behaviour on water infiltration, with a higher remobilization of tracer.

Besides this mean behaviour and the variable effect of snow, plotting the reaction time against the rainfall intensity highlights a clear dependency (Figure 9). The higher the rainfall intensity, the faster the reaction of the percolation. Higher rainfall intensities result in saturation being reached faster in the vadose zone, enabling the activation of fast transfer routes. The slowest velocity estimated for quickflow transits gives values around 10 m/hr, approaching the velocity without rainfall effect. There is a continuum of water transit velocities between the slow—diffuse—mode and the fast—concentrated—mode that activates high permeability routes.
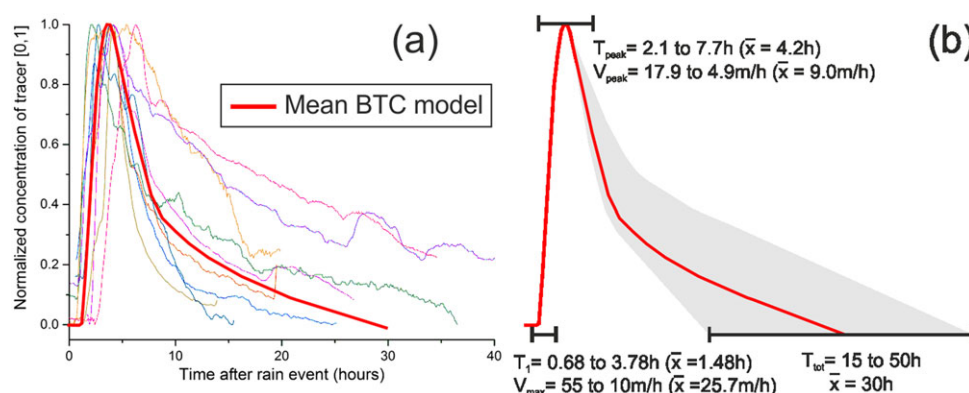
FIGURE 7 (a) Individual breakthrough curves (BTCs) for the 16 rainfall-associated peaks of dye due to quickflow and (b) mean behaviour of the quickflow transport derived from individual BTC
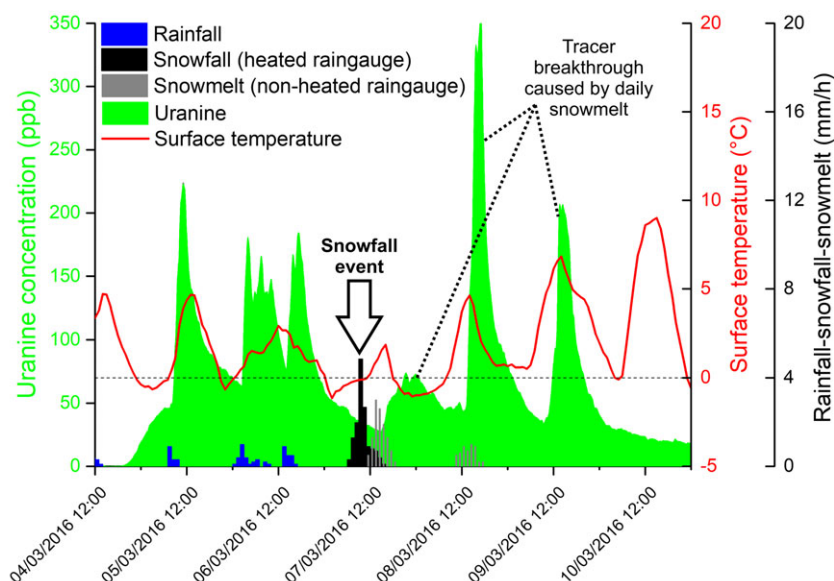
FIGURE 8 Secondary restitution peaks caused by the melting of the snow cover
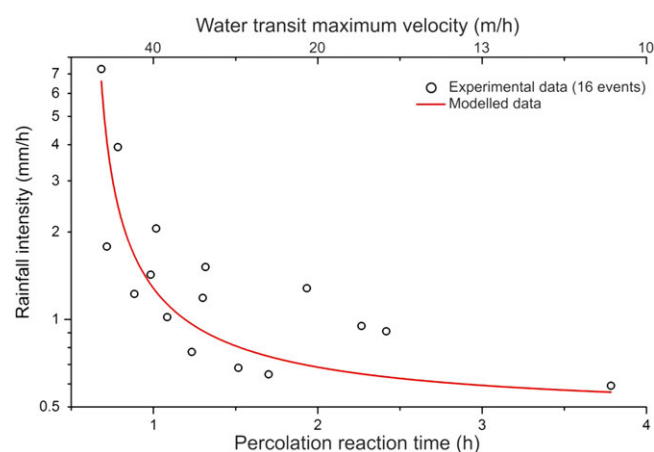
FIGURE 9 Relationship between rainfall intensity of a specific event and reaction time (first arrival) of the dye concentration to this event. Top *X* axis gives the maximum transit velocity between the injection point and percolation in the cave (38 m)

5 | FLOW AND STORAGE MODELLING

5.1 | Conceptual model of karst vadose zone

Experimental results in the Val d'Enfer chamber evidenced multicomponent flow in the vadose zone. Event-related vadose storage is induced from sustained percolation and dye tracing data. A simple two-flow conceptual model is proposed to account for the variable recharge modes highlighted by the field results (Figure 10). This model is similar to the multireservoir models proposed by Sinreich and Flynn (2011), Perrin (2003), and Perrin and Kopp (2005) also for karst vadose zone.

The model should simulate a perennial diffuse flow coming from a slow transit through fine fissures and limestone matrix. This diffuse flow remains active throughout the year, allowing the continuous vadose percolation as seepage flow. By doing so, it represents a significant storage of water in the vadose zone that is recharged by each rainfall event. Infiltration export by this first flow component represents two thirds of the annual recharge, with maximum flow velocities of 10 m/hr and residence times ranging from a few hours to more than

100 days. At the same time, the model has to reproduce the sharp responses of a quickflow transit bypassing the matrix pathways via the concentration of infiltration towards high permeability zones (fissures and shafts). This quickflow component does not recharge vadose zone storage and accounts for one third of the annual aquifer recharge. It has a small transit time (a few hours) and maximum velocities up to 55 m/hr. In this model, the epikarst layer role is mainly to concentrate the infiltration according to the saturation state of downward routes. The input data of the model are effective rainfalls.

5.2 | Discharge simulation

The simulation of the percolation discharge was performed in order to reproduce the dynamic highlighted by experimental approaches. The KarstMod approach developed by the SNO Karst was selected (Jourde, Mazzilli, Lecoq, Arfib, & Bertin, 2015; Mazzilli et al., 2017). It is an adjustable platform for the simulation of rainfall–discharge relationship of karst springs and hydrodynamic analysis. KarstMod reproduces the structure of the conceptual model in order to simulate the discharge on the basis of physical considerations. Further details about the model can be found on the SNO Karst website (www.sokarst.org).

In its complete form, the KarstMod approach is used to simulate karst spring discharges and the hydrodynamic at a catchment scale. Present simulations focus on a simplified form of KarstMod, aiming at simulating the recharge process as illustrated by the conceptual model (Figure 10). The recharge signal is the basis input of KarstMod and is a key variable of such physically based approach (Tritz et al., 2011).

This approach was used by Tritz et al. (2011) with the development of a non-linear hysteretic transfer model that was further implemented in KarstMod. The conceptual behaviour of the vadose zone in Figure 10 is represented by two reservoirs with two possible downward fluxes. The first reservoir (*E*) represents the soil/epikarst that receives effective rainfall (*ER*) and separates infiltration into a quickflow and a diffuse flow. The second reservoir (*V*) represents the vadose storage that is evidenced from field data. The first flux
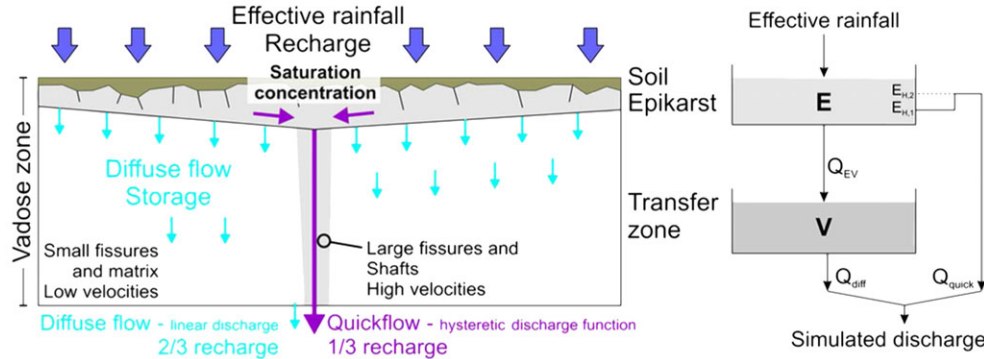
FIGURE 10 Conceptual model of vadose zone hydrological behaviour based on the field data measured in the Val d'Enfer Cave and hysteresis-based model with structure and parameters. E = soil–epikarst reservoir; V = vadose storage reservoir; $E_{H,1}$ and $E_{H,2}$ = hysteretic discharge function thresholds; Q_{EV} = flow component from E to V; Q_{diff} = diffuse flow component; Q_{quick} = quick flow component (modified from Tritz et al., 2011)

characterizes the diffuse flow component through matrix and small fissures, joining the epikarst with the vadose reservoir (Q_{EV}) and then leaking to the outlet from V (Q_{diff}). This flux is the main recharge mode of the karst aquifer. The second flux is a hysteretic discharge law accounting for the variable connectivity in the soil/epikarst zone. As described by Tritz et al. (2011), it represents the fast component of the catchment response to rainfall events allowed by the saturation in the epikarst that activates preferential flowpaths. Here, it is represented by Q_{quick}. The modelled recharge is governed by the balance equations of the reservoirs (Jourde et al., 2015):

$$\frac{dE}{dt} = \begin{cases} ER - Q_{EV} - Q_{quick} & \text{if } E > 0 \\ ER & \text{if } E = 0 \end{cases}, \tag{4}$$

$$\frac{dV}{dt} = Q_{EV} - Q_{diff}. \tag{5}$$

The diffuse discharge Q_{EV} and Q_{diff} is defined with the water level in the reservoirs E and V (mm), specific discharge coefficients k_{EV} and k_{diff} (mm/hr), and the catchment area S (m^2) (Equation 6 and 7).

$$Q_{EV} = k_{EV} \times E \times S, \tag{6}$$

$$Q_{diff} = k_{diff} \times V \times S. \tag{7}$$

The hysteretic discharge function Q_{quick} is defined with the water level in the reservoirs E (mm), the specific discharge coefficient k_{quick} (mm/hr), and the catchment area S (m^2; Equation 8). It is activated if the water level E (mm) reaches a minimum threshold ($E_{H,2}$). This occurs when the epikarst is sufficiently saturated, allowing quickflow activation. $E_{H,1}$ and $E_{H,2}$ standing for the lower and upper threshold levels for the activation of the discharge. This connectivity is represented by ε that is switched to 1 if E rises above $E_{H,2}$ and switched to 0 if E falls below $E_{H,1}$.

$$Q_{quick} = \varepsilon \times k_{quick} \times \left(\frac{E - E_{H,1}}{E_{H,1} - E_{H,2}}\right) \times S, \tag{8}$$

$$\left.\begin{matrix} \varepsilon = 0 \\ E = E_{H,2} \end{matrix}\right\} \rightarrow \varepsilon = 1, \tag{9}$$

$$\left.\begin{matrix} \varepsilon = 1 \\ E = E_{H,1} \end{matrix}\right\} \rightarrow \varepsilon = 0. \tag{10}$$

In their study, Tritz et al. (2011) show the robustness of the hysteretic transfer function to reproduce karst recharge mechanisms. Here, the total modelled discharge for the vadose percolation is the sum of Q_{diff} and Q_{quick} that is compared with the observed discharge. The first discharge event (01/03/2016 to 25/03/2016) was used as a warm-up stage, the calibration of parameters was made on the second and third events (26/03/2016 to 25/05/2016), and the following events were used for validation (26/05/2016 to 15/08/2016). The calibration was performed by adjusting the storage and flow parameters to get the best fit regarding the observed data. The parameters to be calibrated were $E_{H,1}$; $E_{H,2}$; k_{EV}; k_{diff}; k_{quick}; and S. The Nash–Sutcliff efficiency (NSE) coefficient is used as a performance criteria in KarstMod.

$$NSE\left(\sqrt{Q}\right) = \left(1 - \frac{\sum\left(\sqrt{Q_S} - \sqrt{Q_{obs}}\right)^2}{\sum\left(\sqrt{Q_{obs}} - \sqrt{\overline{Q_{obs}}}\right)^2}\right) \times 100 \, (\%). \tag{11}$$

Q_S is the simulated discharge, whereas Q_{obs} is the observed discharge. A NSE of 100% corresponds to a perfect match between model and observation. An efficiency of 0% means that the model performs equally to the mean of observed data. The NSE was calculated on the square root of discharge in order to limit the weight of high-discharge periods on the performance criteria.

Figure 11 shows the results of the simulation with KarstMod and the different stages of modelling. The Table 3 gives the set of model parameters obtained from the calibration period. The simulation gives a NSE of 75.6% for the calibration period and 80.9% for the validation period. Although the overall simulation fits with the observed data, the match could be better (Tritz et al., 2011 obtained NSE > 90%). The model better simulates the quickflow component than the diffuse flow, especially for lower discharge. Some discharge events are not simulated by the model or are too low compared with observed data. This indicate that the two-flow components are probably too simple to account for the variability of flow mechanisms in the vadose zone and interactions between quickflow and diffuse flow.

Nevertheless, model parameters are coherent with literature values in terms of specific discharge coefficients, and the minimum drainage area (56.4 m^2) fits with field observations. Epikarst reservoir thresholds are very low compared with observed or modelled storage in other studies. Tritz et al. (2011) modelled 100 and 119 mm, respectively, for $E_{H,1}$ and $E_{H,2}$, Poulain et al. (2015) measured a threshold of 102 to 139 mm
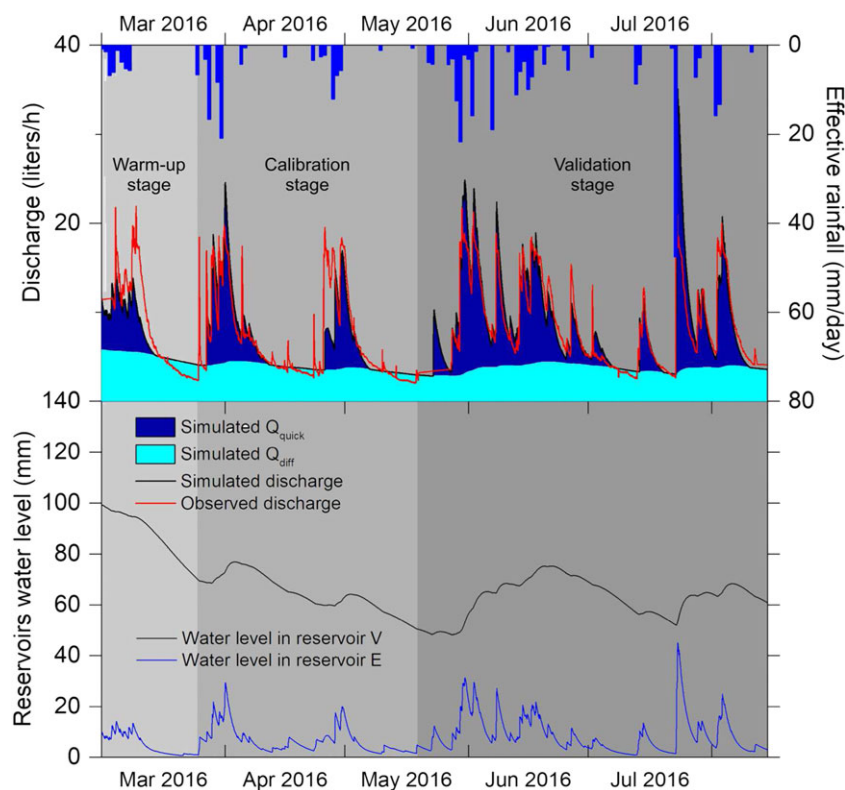
FIGURE 11 Results of the KarstMod simulation for the percolation discharge of the Val d'Enfer with warm-up, calibration, and validation stages. Overall simulation fits to observed data, and the two-flow regime model is able to reproduce the variable recharge modes through the vadose zone. E = soil–epikarst reservoir; V = vadose storage reservoir; Q_diff = diffuse flow component; Q_quick = quick flow component

TABLE 3 Calibration parameters of the KarstMod simulation

Parameters					
$E_{H,1}$ (mm)	$E_{H,2}$ (mm)	k_{EV} (mm/hr)	k_{diff} (mm/hr)	k_{quick} (mm/hr)	S (m²)
2.31	5.79	0.008	0.001	0.013	56.4

for the epikarst reservoir, and Arbel et al. (2010) estimated this value to be 120 mm. The value at the Rochefort Cave site indicates a quick saturation of the epikarst leading to a limited storage behaviour. However, the simulated level in the vadose storage shows that a significant volume of water (50 to 70 mm) may be stored by the diffuse flow component allowing an event-based storage.

These results are promising to obtain reliable physically based model to simulate variable recharge processes through the karst vadose zone based on rainfall data. Simple models are not suited to simulate the complexity of vadose processes influenced by local features. However, a large part of vadose discharge variability can be explained based on effective precipitation, leading to a resolved evaluation of recharge signal in the karst system.

Sensitivity analysis was performed on the calibration parameters to evaluate the variance that can be attributed to each parameter taken singularly. The sensitivity index S_i for parameter X_i with respect to the simulated discharge Q_S is defined as the fraction V_i of the variance $V(Q_S)$ of the simulated discharge which is due solely to the parameter X_i (KarstMod user guide, 2017).

$$S_i = \frac{V_i}{V(Q_S)}. \tag{12}$$

S_i is calculated using the Sobol procedure described by Saltelli (2002). KarstMod provides the sensitivity indexes based on

$N = 1000 * (n_{par} + 2)$ parameters sets, where n_{par} is the number of parameters to be calibrated. S_i allows estimating the influence of parameters on model output and thus detecting overparameterization. Table 4 displays the sensitivity index calculated for the eight parameters of the model. The upper and lower threshold levels of the hysteretic transfer function are the most sensitive parameters (0.442 and 0.105, respectively) which show the importance of this mechanism in the percolation behaviour. Initial levels in the reservoirs (E_0 and V_0) have almost no influence on the simulated discharge which show that the warm-up period is long enough.

6 | DISCUSSION

6.1 | Recharge dynamic quantification through karst vadose zone

The data measured in the Rochefort Cave fit with the classical conception of recharge through karst vadose zone where the percolation discharge can be considered as the combination of quickflow and diffuse

TABLE 4 Individual parameter sensitivity indexes

Parameters	First-order index
$E_{H,2}$	0.442
$E_{H,1}$	0.105
k_{diff}	0.096
k_{quick}	0.038
k_{EV}	0.035
V_0	0.020
S	0.007
E_0	0.0005

flow components (Arbel et al., 2008; Arbel et al., 2010; Bakalowicz, 1995; Hartmann et al., 2014; Perrin, 2003; Sheffer et al., 2011; Trcek, 2007). Diffuse flow is the slow recharge component through small fissures and matrix, leading to sustained percolation. Quickflow is the fast infiltration taking place in high permeability zones activated by saturation and leading to bypass.

Hydrograph separation based on recession characteristics allows the identification of the two-flow recharge dynamic. In a similar approach, Arbel et al. (2008) used this method to separate hydrograph components on drip rates and found that the recession constant was variable and depended on previous wetness of the vadose zone. Here, the regularity of the recession processes in spring and summer 2016 shows a minimal influence of preevent conditions or evapotranspiration. This allows a separation of the flow components throughout the year together with an estimation of their respective volumes and roles in the recharge process. The same approach was used by Smart and Friederich (1987) and recently by Liu, Brancelj, and Burnet (2016). They show how recession analyses may be applied on vadose flows to derive storage characteristics of different flow components. Sheffer et al. (2011) also pointed specific flow components based on hydrograph recessions. They identified the repetition in recession flow regimes as indicators for a recharge governed by vadose zone characteristics. This repetition in recession behaviour is visible in the present data, giving the opportunity to derive vadose zone characteristics and quantify the respective flow regimes.

In the Rochefort Cave, a major part (two thirds) of the recharge is diffuse infiltration through the limestone matrix and small fissures. This component has a recession constant longer than 10 days and a low recession coefficient. A mean transit velocity of 1 m/hr has been calculated based on dye tracing. This is in accordance with mean velocities of 0.88 m/hr calculated in the same geological context (Poulain et al., 2015). It is also in agreement with velocity values found in other karst systems (Allshorn, Bottrell, West, & Odling, 2007; Arbel et al., 2010; Kogovsek, 2010; Sheffer et al., 2011). This diffuse flow component has a residence time in the vadose zone longer than 15 days and can be considered as an event-water storage because the slow transit causes significant retardation to recharge.

Alternatively, the remaining one third of the recharge is made through a fast flow infiltration (quickflow) concentrated by epikarst towards high permeability zones. This bottleneck effect is a major role of the epikarst (Perrin, 2003; Williams, 2008). During rainfall events, shafts and open fractures efficiently drain a large part of the rainfall infiltration. This fast component exhibits velocities of more than 10 m/hr, up to 55 m/hr. The dye tracing indicates that the intensity of the rainfall event influences the transit velocity. The role of previous conditions in the system was not evidenced as an influencing factor for infiltration velocity in this case. This indicates a short residence time of water in the epikarst (<3 days) that does not allow significant storage to maintain a saturation state. Intense rainfall triggers the most effective recharge process as it quickly activates high permeability zones. A similar relationship between intensity and transit velocity was evidenced by Chevalier (1988), being now clearly quantified. Successive quickflow events have similar characteristics based on the remobilization of solute that they caused, as identified by the dye tracing. This confirms the statement that vadose zone characteristics

govern the recharge process, from the diffuse flow component to the quickflow. The mean behaviour based on secondary BTC gives the average transit characteristics under quickflow conditions.

The EC and temperature of percolation water confirm the hypothesis based on hydrograph separation. Temperature analysis highlighted a two-component recharge process in this vadose zone. The major part of the temperature signal is governed by the slow transit of the water through low permeability parts of the vadose zone (3 to 6-hr lag with surface). This gives a highly damped signal coming from prolonged residence time and mixing with storage water. When quickflow recharge is active, influence of surface temperature is quickly transferred and much stronger due to the lower dilution factor and the activation of bypass routes into the vadose zone. EC measurement itself cannot be used to perform hydrograph separation because of its nonconservative behaviour (Bakalowicz, 1995; Jeannin et al., 2007; Perrin, 2003). However, variations of EC are useful to evaluate the presence of freshwater (low EC) in the percolation signal. The limited importance of quickflow in the overall recharge volume meets the conclusions of Arbel et al. (2010) that used chloride concentration for hydrograph separation. They evidenced the low percentage (15–22%) of preferential water relative to "old water" in vadose flow. Nevertheless, this study, as many authors, evidence the ability of quickflow to accommodate high recharge rate, hence to have a high contribution to the overall aquifer recharge (Smart & Friederich, 1987).

Simulations using a two-flow recharge model enable to simulate the percolation behaviour measured in the Val d'Enfer. The hysteretic transfer function developed by Tritz et al. (2011) and applied in KarstMod can reproduce the specific behaviour of the uppermost part of the karst vadose zone. Our case study shows that variable and local recharge processes can and must be accounted for to model the behaviour of karst aquifers' responses to rainfall. Recharge efficiency seems to be strongly dependent on the intensity of recharge but also on the type of precipitation.

6.2 | Implications for karst aquifer vulnerability

Dye tracing highlights the vulnerability of the karst aquifer regarding surface contamination. Infiltration through vadose zone is fast despite any evidence for preferential infiltration points. One should note that the low recovery rate of the dye allows only a partial analysis of the vadose hydrodynamic. Nevertheless, such a low value is not unusual for vadose dye tracing. Allshorn et al. (2007) obtained 0.004% in chalk, Arbel et al. (2008) had less than 1% in Mediterranean karst, Kogovsek's (2010) recovery rates were generally less than 0.2% in Slovenian caves, and Poulain et al. (2015) obtained 0.013% in the same geological context. The low recovery rate highlights the large dispersion of dye in the vadose zone driven by the diffusive transport spreading the recharge water.

Separation of the BTC in two transit modes was possible due to the strong restitution contrast between those modes and high resolution monitoring. On the one hand, diffuse recharge represents 40% of the measured tracer at the percolation. It shows a slow transit with a very long total restitution time (more than 120 days). This mode of transit results in strong diffusion/dilution processes and thus in the attenuation of solute concentrations. Nevertheless, prolonged tail of

the BTC shows that slow infiltration and storage will cause extended residence time of solute. On the other hand, the quickflow mode is responsible for a faster and concentrated transport of solute. It represents 60% of the recovered solute at the percolation. This mode concentrates the drainage towards high permeability zones and also results in a strong remobilization of solute. This mode of transmission limits a possible attenuation of solute as it concentrates the infiltration.

Here, the progressive concentration decrease of quickflow remobilization shows how successive activations of quickflow by epikarst saturation generate a dilution and mixing process in a given vadose zone volume. Results of snowmelt effect on remobilization evidenced a stronger influence. This highlights that rainfall and snowfall must be considered separately when dealing with groundwater recharge.

7 | CONCLUSIONS

The main goal of this experimental study was to identify and quantify recharge modes through the vadose zone of karst aquifers by in situ approaches in the Rochefort Cave (Belgium). Based on this quantification, the question of their impact on recharge efficiency and aquifer vulnerability has been investigated. Both discharge monitoring and artificial dye tracing highlighted a two-flow component behaviour with a continuous diffuse recharge and an ephemeral quickflow recharge. This agrees with field results coming from vadose percolation described in similar experimental researches.

Recharge processes through karst vadose zone can be described as the relative contribution of sustained diffuse flow through lower permeability zones and ephemeral quickflow concentrated towards high permeability pathways. Local scale approach using vadose percolation monitoring, dye tracing, and physically based simulations gives a quantitative assessment of the recharge modes, their characteristics, and efficiencies regarding precipitation transfers to phreatic zone. On the present case, the majority of the infiltration water is transferred through diffuse and slow infiltration, delaying aquifer recharge with a significant storage of water. On the other hand, rainfall events and quick saturation of slow permeability downward routes create a quickflow recharge bypassing usual drainage in concentrated flows. Epikarst acts as a shunting area, distributing infiltration according to saturation with a very short-time storage potential. These results have two implications regarding the karst aquifer resource.

First, it is necessary to better define and quantify recharge processes using regional scale approaches. As climate change appears to impact precipitation patterns due to temperature changes, rainfall intensity is expected to increase in many parts of the world (Singh, Arya, Taxak, & Vojinovic, 2016; Wang et al., 2017). Thus, the evidence for a rainfall intensity and snowmelt effect on the recharge efficiency is of particular concern for karst aquifers. More intense precipitations and possible modifications of precipitation type (rainfall or snowfall) will affect the recharge process of karst aquifers in quantitative and qualitative ways. Faster infiltration triggered by high intensity rainfalls will enhance aquifer recharge but also its vulnerability. In regions where karst groundwater supply a major part of the drinkable water,

how will future conditions of rainfall intensity, evapotranspiration, or snow cover affect karst groundwater as a resource?

Second, karst aquifer contamination assessment strongly relies on the variable recharge mode. Dominance of either quickflow or diffuse recharge and the importance and location of storage will impact the fate of contaminant over a karst area. Quantification of transit characteristics and residence time in the hydrological system is the only way to properly address potential contamination issues. Complementary methodologies based on near-surface geophysic monitoring are being used to precise this hydrogeological approach (Watlet, Kaufmann, Francis, & Van Camp, 2015; Van Camp et al., 2016, Watlet et al., 2018).With the growing anthropogenic pressure on groundwater, maintaining water quality is a challenging task, even more in karst regions.

Present study was intentionally spatially limited and cannot be integrated over a regional area or catchment given the spatial and temporal variability of karst features. Nevertheless, it highlights recharge processes and their relative importance in the hydrological processes of karst vadose zone. Integrative approaches give a complementary view on the hydrological processes and their meaning with respect to aquifer recharge and the future management of karst groundwater resources.

ORCID

Amaël Poulain http://orcid.org/0000-0001-5202-7588
Arnaud Watlet http://orcid.org/0000-0003-0318-9032
Michel Van Camp http://orcid.org/0000-0002-2859-3122
Naomi Mazzilli http://orcid.org/0000-0002-9145-5160

REFERENCES

Allen, R., Pereira, L., Raes, D., Smith, M. (1998). Crop evapotranspiration—Guidelines for computing crop water requirements—FAO irrigation and drainage paper 56. FAO, Rome.

Allshorn, S., Bottrell, S., West, L., & Odling, N. (2007). Rapid karstic bypass flow in the unsaturated zone of the Yorkshire chalk aquifer and implications for contaminant transport. In M. Parise, & J. Gunn (Eds.), *Natural and anthropogenic hazards in karst areas: Recognition, analysis and mitigation. Geological Society, Longon, Special Publications, 279* (pp. 111–122).

Aquilina, L., Ladouche, B., & Doerfliger, N. (2005). Recharge processes in karstic systems investigated through the correlation of chemical and isotopic composition of rain and spring-waters. *Applied Geochemistry, 20*, 2189–2206.

Aquilina, L., Ladouche, B., & Doerfliger, N. (2006). Water storage and transfer in the epikarst of karstic systems during high flow periods. *Journal of Hydrology, 327*, 472–485.

Arbel, Y., Greenbaum, N., Lange, J., & Inbar, M. (2010). Infiltration processes and flow rates in developed karst vadose zone using tracers in cave drips. *Earth Surf. Proc. Land., 35*, 1682–1693.

Arbel, Y., Greenbaum, N., Lange, J., Shtober-Zisu, N., Grodek, T., Wittenberg, L., & Inbar, M. (2008). Hydrologic classification of cave drips in a Mediterranean climate, based on hydrograph separation and flow mechanisms. *Israel Journal of Earth Sciences, 57*, 291–310.

Bakalowicz, M. (1979). Contribution de la géochimie des eaux à la connaissance de l'aquifère karstique et de la karstification. Doctorat ès Sciences naturelles thesis, P. et M. Curie Paris-6 University, 269p.

Bakalowicz, M. (1995). The infiltration zone of karst aquifers. Investigation methods, structure and behavior. *Hydrogéologie, 4*, 3–21.

Bakalowicz, M. (2013). Epikarst Processes. In: Shroder J (editor in chief), Frumkin A (ed), *Treatise on geomorphology*. Academic Press, San Diego, CA, vol. 6, Karst Geomorphology, 164–171.

Bakalowicz, M., Blavoux, B., & Mangin, A. (1974). Apport du traçage isotopique naturel à la connaissance du fonctionnement d'un système karstique. *Journal of Hydrology, 23*, 141–158.

Baker, A., & Brunsdon, C. (2003). Non-linearities in drip water hydrology: An example from stump cross caverns, Yorkshire. *Journal of Hydrology, 277*, 151–163.

Barchy, L., Dejonghe, L., Marion, J-M. (2014). Rochefort – Nassogne n°59/3–4, Carte géologique de Wallonie. SPW – DGARNE.

Behrens, H., Benischke, R., Bricelj, M., Harum, T., Käss, W., Kosi, G., … Zupan, M. (1992). Investigations with natural and artificial tracer in the karst aquifer of the Lurbach system (Peggau-Tanneben-Semriach, Austria). *Steir. Beitrh. Z. Hydrogeologie, 43*, 9–158.

Birkhoff, E., Bollaert, R., Burgers, J., de Graauw, L., Dikstra, M., Legros, M., De Sadelaer, G., Schaballie, S. (2013). Nouvelle topographie de la Grotte du Nou Maulin, http://noumaulin.blogspot.com

Bottrell, S., & Atkinson, T. (1992). Tracer study of flow and storage in the unsaturated zone of a karstic limestone aquifer. In H. Höltz, & A. Werner (Eds.), *Tracer Hydrology* (pp. 207–211). Rotterdam: Balkema.

Bultynck, P., & Dejonghe, L. (2001). Devonian lithostratigraphic units (Belgium). In: Bultynck, P., Dejonghe, L. (eds), guide to a revisited lithostratigraphic scale of Belgium. *Geologica Belgica, 4*, 39–69.

Van Camp, M., Watlet, A., Poulain, A., Hallet, V., Rochez, G., Quinif, Y., Meus, P., Francis, O., Kaufmann, O. (2016). Continuous gravimetric monitoring as an integrative tool for exploring hydrological processes in the Lomme Karst System (Belgium). AGU Fall Meeting 2016, San Francisco, USA.

Fu, Z., Chen, H., Xu, Q., Jia, J., Wang, S., & Wang, K. (2016). Role of epikarst in near-surface hydrological processes in a soil manteled subtropical dolomite karst slope: Implications of field rainfall simulation experiments. *Hydrological Processes, 30*, 795–811. https://doi.org/10.1002/hyp.10650

Chevalier, J. (1988). *Hydrodynamique de la zone non saturée d'un aquifère karstique: étude expérimentale*. Thèse de doctorat: Université de Montpellier II. 212p

De Block, G. (1972). Les grottes les plus longues et les abîmes les plus profonds de Belgique. *Bull Inf. Equipe Spéléo Brux. Belg., 52*, 18–24.

Dehove, J., Nandance, J.-L., Renier, J-M. (1978). Topographie de la grotte de Lorette, S.C. Rochefortois.

Deville, S. (2013). *Caractérisation de la zone non saturée des karsts par la gravimétrie et l'hydrogéologie*. Thèse de doctorat: Université Montpellier II. 241p

Ford, D., & Williams, P. (2007). *Karst hydrogeology and geomorphology*. London: John Wiley & Sons.

Genty, D., & Deflandre, G. (1998). Drip flow variation under a stalactite of the Père Noël cave (Belgium). Evidence of seasonal variation and air pressure constraints. *Journal of Hydrology, 211*, 208–232.

Gunn, J. (1983). Point-recharge of limestone aquifers—A model from new-Zealand karst. *Journal of Hydrology, 61*, 19–29.

Hartmann, A., Goldscheider, N., Wagener, T., Lange, J., & Weiler, M. (2014). Karst water resources in a changing world: Review of hydrological modeling approaches. *Reviews of Geophysics, 52*, 218–242.

Hartmann, A., Lange, J., Weiler, M., Arbel, Y., & Greenbaum, N. (2012). A new approach to model the spatial and temporal variability of recharge to karst aquifer. *Hydrology and Earth System Sciences, 16*, 2219–2231.

Hunkeler, D., & Mudry, J. (2007). Hydrochemical methods. In N. Goldscheider, & D. Drew (Eds.), *Methods in karst hydrogeology*. International contribution to hydrogeology (pp. 93–122). London: Taylor & Francis.

Jacob, T., Bayer, R., Chery, J., Jourde, H., Le Moigne, N., Boy, J.-P., … Brunet, P. (2008). Absolute gravity monitoring of water storage variation in a karst aquifer of the Larzac plateau (Southern France). *Journal of Hydrology, 359*, 105–117.

Jeannin, P.-Y., Groves, C., & Häuselaman, P. (2007). Speleological investigations. In N. Goldscheider, & D. Drew (Eds.), *Methods in karst hydrogeology* (pp. 25–44). London: Taylor & Francis.

Jocson, J., Jenson, J., & Contractor, D. (2002). Recharge and aquifer response: Northern Guam Lens Aquifer, Guam, Mariana Islands. *Journal of Hydrology, 260*, 231–254.

Jones, W., Culver, D., & Herman, J. (2004). *Epikarst*. Special Publication 9. Charles Town, WV: Karst Water Institute.

Jourde, H., Mazzilli, N., Lecoq, N., Arfib, B., & Bertin, D. (2015). KARSTMOD: A generic modular reservoir dedicated to spring discharge modeling and hydrodynamic analysis in karst. In B. Andreo, F. Carrasco, J. Duran, P. Jimenez, & J. LaMoreaux (Eds.), *Hydrogeological and environmental investigations in karst systems, Environmental Earth Sciences* (Vol. 1) (pp. 35–43).

KarstMod user guide (2017). KarstMod used guide version 2.0 (2017/05). SNO Karst. http://www.sokarst.org/

Kaufmann, O., Bastin, C., Barcella, C., Watlet, A., Van Ruymbeke, M. (2016) design and calibration of a system for monitoring highly variable dripwater flows in cave. 5th Unternational Geologica Belgica meeting 2016, Mons, Belgium.

Klimchouk, A. (2004). Towards defining, delimiting and classifying epikarst: Its origin, processes and variants of geomorphic evolution. In W. Jones, D. Culver, & J. Herman (Eds.), *Epikarst. Special Publication 9. Karst Water Institute* (pp. 23–35).

Klimchouk, A., Sauro, U., & Lazzarotto, M. (1996). "Hidden" shafts at the base of the epikarstic zone: A cause study from the Sette Communi plateau, Venetian Pre-Alps, Italy. *Cave and karst. Science, 23*, 101–107.

Kogovsek, J. (1997). Water tracing test in vadose zone. In Y. A. Kranjc (Ed.), *Tracer Hydrology 97* (pp. 167–172). Rotterdam: Balkema.

Kogovsek, J. (2010). *Characteristics of percolation through karst vadose zone*. Postojna-Ljubljana: ZRC Publishing.

Kogovsek, J., & Petric, M. (2014). Solute transport processes in a karst vadose zone characterized by long-term tracer tests (the cave system of Postojska Jama, Slovenia). *Journal of Hydrology, 519*, 1205–1213.

Kullman, E. (1990). *Karst fissure waters (in Slovak)*. Bratislava: Geologicky ustav Dionyza Stura. 184p

Legros, M. (2000). Topographie de la Nouvelle Galerie de la Grotte de Lorette, S.C. Les Fistuleuses.

Liu, A., Brancelj, A., & Burnet, J. (2016). Interpretation of epikarstic cave drip xwater recession curves: A case study from Velika Pasica Cave, Central Slovenia. *Hydrological Sciences Journal, 61*, 2754–2762. https://doi.org/10.1080/02626667.2016.1154150

Maillet, E. (1905). Essais d'hydraulique souterraine et fluvatile. Vol 1. Herman et Cie, Paris, 218p.

Malik, P. (2015). Evaluting discharge regimes of karst aquifer. In Z. Stevanovic (Ed.), *Karst aquifers—Characterization and engineering*. Professional Practice in Earth Sciences (2015) (pp. 205–249).

Mangin, A. (1975). Contribution à l'étude hydrodynamique des aquifères karstiques. Doctorat ès Sciences naturelles, Université de Dijon. In : Ann. Spéléol., 29, 283–332, 795–601; 30, 21–124.

Markowska, M., Baker, A., Treble, P., Andersen, M., Hankin, S., Jex, C., … Roach, R. (2015). Unsaturated zone hydrology and cave drip discharge water response: Implications for speleothem paleoclimate record variability. *Journal of Hydrology*, 529, 662–675. https://doi.org/10.1016/j.jhydrol.2014.12.044

Mazzilli, N., Guinot, V., Jourde, H., Lecoq, N., Labat, D., Arfib, B., … Bertin, D. (2017). KarstMod: A modelling platform for rainfall—Discharge analysis and modelling dedicated to karst systems. *Environmental Modelling and Software*. https://doi.org/10.1016/j.envsoft.2017.03.015

Mudarra, M., & Andreo, B. (2011). Relative importance of the saturated and the unsaturated zones in the hydrogeological functioning of karst aquifers: The case of Alta Cadena (Southern Spain). *Journal of Hydrology*, 379, 263–280. https://doi.org/10.1016/j.jhydrol.2010.12.005

Perrin, J. (2003). *A conceptual model of flow and transport in a karst aquifer based on spatial and temporal variations of natural tracers*. PhD thesis, University of Neuchâtel, 227p.

Perrin, J., & Kopp, L. (2005). Hétérogénéité des écoulements dans la zone non saturée d'un aquifère karstique (site de Milandre, Jura suisse). Bulletin d'Hydrogéologie. 21, 22–58.

Pipan, T., & Culver, D. (2007). Copepod distribution as an indicator of epikarst system connectivity. *Hydrogeology Journal*, 15, 817–822.

Poulain, A., Rochez, G., Bonniver, I., & Hallet, V. (2015). Stalactite drip-water monitoring and tracer tests approach to assess hydrogeologic behavior of karst vadose zone: Case study of Han-sur-Lesse (Belgium). *Environment and Earth Science*, 74, 7685–7697.

Poulain, A., Rochez, G., Van Roy, J.-P., Dewaide, L., Hallet, V., & De Sadelaer, G. (2017). A compact field fluorimeter and its application to dye tracing in karst environments. *Hydrogeology Journal*, 25, 1517–1524.

Pronk, M., Goldscheider, N., Zopfi, J., & Zwahlen, F. (2009). Percolation and particle transport in the unsaturated zone of a karst aquifer. *Ground Water*, 47, 361–369.

Quinif, Y., & Vandycke, S. (2001). Les phénomènes karstiques de la région de Han-sur-Lesse (Belgique). *Bull. Inf. Bass. Paris*, 38, 6–19.

Rouch, R. (1964). Sur le peuplement des grottes par certaines espèces de Copépodes. *Speleunca Mémoires*, 4, 200–201.

Rouch, R. (1968). Contribution à la connaissance des Harpacticoïdes hypogés (Crustacés, Copépodes). *Ann. Spéléol.*, 23, 5–167.

Saltelli, A. (2002). Making best use of model evaluations to compute sensitivity indexes. *Computer Physics Communications*, 145, 280–297.

Sauter, M. (1992). Quantification and forecasting of regional groundwater flow and transport in a karst aquifer (Gallusquelle, Malm, SW. Germany). Tübinger Geowisenschaftliche Arbeiten, C13.

Sheffer, N., Cohen, M., Morin, E., Grodek, T., Gimburg, A., Magal, E., … Frumkin, A. (2011). Integrated cave drip monitoring for epikarst recharge estimation in a dry Mediterranean area, Sif Cave, Israel. *Hydrological Processes*, 25, 2837–2845.

Singh, R., Arya, D. S., Taxak, A. K., & Vojinovic, Z. (2016). Potential impact of climate change on rainfall intensity-duration-frequency curves in Roorkee, India. *Water Resources Management*, 30, 4603–4616.

Sinreich, M., Flynn, R. (2011). Comparative tracing experiments to investigate epikarst structural and compositional heterogeneity. Speleogenesis and Evolution of Karst Aquifers, Issue 10.

Smart, P., Friederich, H. (1987). Water movement and storage in the unsaturated zone of a maturely karstified carbonate aquifer, Mendip Hills, England. In *Proceeding of the Environmental Problems in Karst Terranes and their solutions Conference*, KY, USA, 57–87.

Trcek, B. (2005). The use of natural tracers in the study of the unsaturated zone of a karst aquifer. *Geologija*, 48, 141–152.

Trcek, B. (2007). Ho can epikarst zone influence the karst aquifer hydraulic behavior? *Environmental Geology*, 51, 761–765. https://doi.org/10.1007/s00254-006-0387-x

Triantafyllou, A., Watlet, A., Kaufmann, O., Le Mouélic, S. (2016). *Exploring structures of the Rochefort Cave (Belgium) with 3D models from LIDAR scans and UAV photoscans*. AGU Fall Meeting 2016, San Francisco, USA.

Tritz, S., Guinot, V., & Jourde, H. (2011). Modelling the behavior of a karst system catchment using a non-linear hysteretic conceptual model. *Journal of Hydrology*, 397, 250–262.

Wang, G., Wang, D., Trenberth, K. E., Erfanian, A., Yu, M., Bosilovich, M. G., & Parr, D. T. (2017). The peak structure and future changes of the relationships between extreme precipitation and temperature. *Nature Climate Change*, 7, 268–274.

Watlet, A., Kaufmann, O., Francis, O., Van Camp M. (2015). *Groundwater storage in a karst vadose zone evidenced using gravimetric and surface-to-borehole ERT monitoring systems*. 21st European Meeting of Environmental and Engineering Geophysics, Turin, Italy.

Watlet, A., Kaufmann, O., Triantafyllou, A., Poulain, A., Chambers, J. E., Meldrum, P. I., … Van Camp, M. (2018). Imaging groundwater infiltration dynamics in karst vadose zone with long-term ERT monitoring. *Hydrology and Earth System Sciences*, 1–42. https://doi.org/10.5194/hess-2017-477

Willems, L., Ek, C., & Marion, J.-M. (2011). Le système karstique de Lomme, région de Rochefort, Cadre général. *Geological Survey of Belgium Professional Paper*, 309, 5–10.

Williams, P. (1983). The role of the subcutaneous zone in karst hydrology. *Journal of Hydrology*, 61, 45–67.

Williams, P. (2008). The role of epikarst in karst and cave hydrology: A review. *International Journal of Speleology*, 37, 1–10.

SUPPORTING INFORMATION

Additional supporting information may be found online in the Supporting Information section at the end of the article.